

Supporting Information

Determining the Spheroid Geometry of Individual Metallic Nanoparticles by Two-Dimensional Single-Particle Dynamic Light Scattering

Luis F. Guerra, Tom W. Muir, and Haw Yang*

*Department of Chemistry, Princeton University, Frick Laboratory, Princeton, New Jersey
08544, United States*

E-mail: hawyang@princeton.edu

Contents

1	<i>W</i> Functions	3
2	Indeterminate Values	3
3	Supplementary Figures	4

List of Figures

S1	Error from Truncation of Infinite Series for $A_{\delta\chi}$	4
S2	$(A_{\delta\chi}, A_{\delta\chi_s})$ vs. Particle Geometry and ξ	4

1 W Functions

The W functions in eqs. (6) and (7) of the text are given by

$$\begin{aligned}
W_{11x}(t, \lambda) &= \frac{1}{4} [2(A + B)(3 + H) - [A + 3AH + 4B(1 + H) + 4C(1 + H) \cos 2\phi(t)] \sin^2 \theta(t) \\
&\quad + (1 + 3H) [B + C \cos 2\phi(t)] \sin^4 \theta(t)] \\
W_{13x}(t, \lambda) &= \frac{1}{16} (1 + 3H) [B + C \cos 2\phi(t)] \sin^2 2\theta(t) \\
W_{33x}(t, \lambda) &= \frac{1}{4} [2 - 2H + (1 + 3H) \sin^2 \theta(t)] \{A + [B + C \cos 2\phi(t)] \sin^2 \theta(t)\} \\
W_{11y}(t, \lambda) &= \frac{1}{4} [2(A + B)(3 + H) - [A + 3AH + 4B(1 + H) - 4C(1 + H) \cos 2\phi(t)] \sin^2 \theta(t) \\
&\quad + (1 + 3H) [B - C \cos 2\phi(t)] \sin^4 \theta(t)] \\
W_{13y}(t, \lambda) &= \frac{1}{16} (1 + 3H) [B - C \cos 2\phi(t)] \sin^2 2\theta(t) \\
W_{33y}(t, \lambda) &= \frac{1}{4} [2 - 2H + (1 + 3H) \sin^2 \theta(t)] \{A + [B - C \cos 2\phi(t)] \sin^2 \theta(t)\}
\end{aligned} \tag{S1}$$

where $A = (1/6) - (1/4) \cos \Theta_s(\lambda) + (1/12) \cos^3 \Theta_s(\lambda)$, $B = (1/8) \cos \Theta_s(\lambda) - (1/8) \cos^3 \Theta_s(\lambda)$, $C = (7/48) - (1/16) \cos \Theta_s(\lambda) - (1/16) \cos^2 \Theta_s(\lambda) - (1/48) \cos^3 \Theta_s(\lambda)$, and $H = \cos [2\Theta_i(\lambda)]$. The explicit wavelength-dependence of the constants A , B , C , and H were omitted for clarity.

2 Indeterminate Values

The indeterminate values (marked as grey) in figs. 4–6 came from two different sources:

1. The maximum-likelihood estimation (MLE) fitting used to calculate the autocorrelation amplitudes did not converge. This was due to excessive noise in the autocorrelation functions, more prevalent at lower SNR values and lower shape parameters.
2. Simulations in which the MLE fitting converged but any calculated decay times for the autocorrelation curves deviated more than 30% from the expected value of $\bar{\tau}_R = 33.3$ were also set as indeterminate. These were values for which calculations of P became unreliable, often occurring at values of λ_{rme} far from the LSPR wavelength and thus poorly positioned for interrogating the spectral contrast.

3 Supplementary Figures

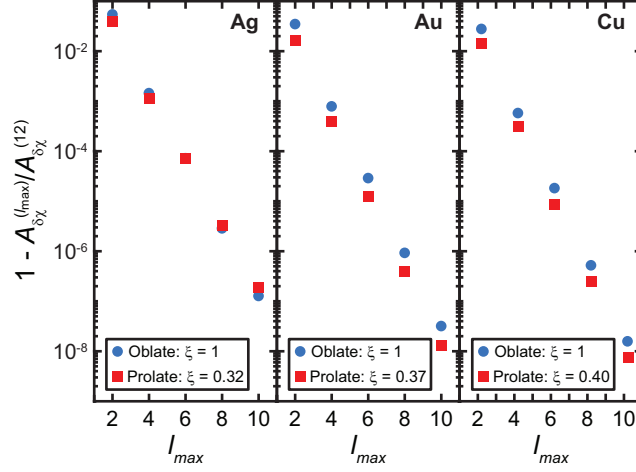


Figure S1: Plots of the truncation error in $A_{\delta\chi}$ as a function of l_{\max} , relative to the value of $A_{\delta\chi}$ with $l_{\max} = 12$, assuming either oblate (filled, blue circles) or prolate (filled, red squares) geometries with the indicated shape parameters and for silver (left panel), gold (middle panel), and copper (right panel) particles. l_{\max} refers to the maximum value of l in the partial sum. Note that only the largest values of ξ_o and ξ_p present in the simulations were needed to find the maximal error contribution from truncation as this error monotonically increases with the shape parameter assuming either geometry.

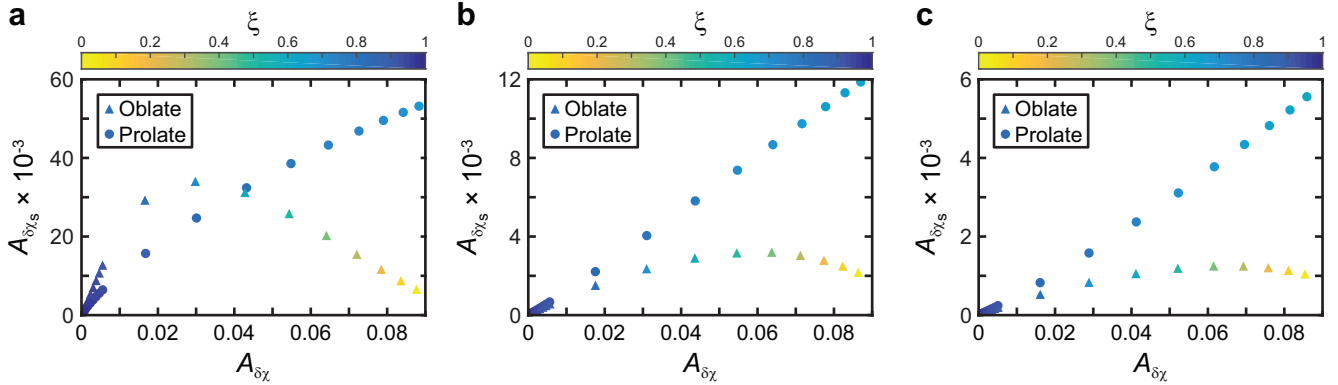


Figure S2: Plots of $(A_{\delta\chi}, A_{\delta\chi_s})$ as a function of particle geometry (oblate - filled triangles; prolate - filled circles) and ξ (color gradient) for (a) silver, (b) gold, and (c) copper particles. Data are taken from the columns in BLAH at the optimal longpass dichroic edge wavelengths: 400 nm, 535 nm, and 510 nm for silver, gold, and copper, respectively.